

# Highly stretchable and tough hydrogels

Jeong-Yun Sun<sup>1,2</sup>, Xuanhe Zhao<sup>3</sup>, Widusha R. K. Illeperuma<sup>1</sup>, Ovijit Chaudhuri<sup>1</sup>, Kyu Hwan Oh<sup>2</sup>, David J. Mooney<sup>1,4</sup>, Joost J. Vlassak<sup>1</sup> & Zhigang Suo<sup>1,5</sup>

Hydrogels are used as scaffolds for tissue engineering<sup>1</sup>, vehicles for drug delivery<sup>2</sup>, actuators for optics and fluidics<sup>3</sup>, and model extracellular matrices for biological studies<sup>4</sup>. The scope of hydrogel applications, however, is often severely limited by their mechanical behaviour<sup>5</sup>. Most hydrogels do not exhibit high stretchability; for example, an alginate hydrogel ruptures when stretched to about 1.2 times its original length. Some synthetic elastic hydrogels<sup>6,7</sup> have achieved stretches in the range 10–20, but these values are markedly reduced in samples containing notches. Most hydrogels are brittle, with fracture energies of about  $10 \text{ J m}^{-2}$  (ref. 8), as compared with  $\sim 1,000 \text{ J m}^{-2}$  for cartilage<sup>9</sup> and  $\sim 10,000 \text{ J m}^{-2}$  for natural rubbers<sup>10</sup>. Intense efforts are devoted to synthesizing hydrogels with improved mechanical properties<sup>11–18</sup>; certain synthetic gels have reached fracture energies of 100–1,000  $\text{J m}^{-2}$  (refs 11, 14, 17). Here we report the synthesis of hydrogels from polymers forming ionically and covalently crosslinked networks. Although such gels contain  $\sim 90\%$  water, they can be stretched beyond 20 times their initial length, and have fracture energies of  $\sim 9,000 \text{ J m}^{-2}$ . Even for samples containing notches, a stretch of 17 is demonstrated. We attribute the gels' toughness to the synergy of two mechanisms: crack bridging by the network of covalent crosslinks, and hysteresis by unzipping the network of ionic crosslinks. Furthermore, the network of covalent crosslinks preserves the memory of the initial state, so that much of the large deformation is removed on unloading. The unzipped ionic crosslinks cause internal damage, which heals by re-zipping. These gels may serve as model systems to explore mechanisms of deformation and energy dissipation, and expand the scope of hydrogel applications.

Certain synthetic hydrogels exhibit exceptional mechanical behaviour. A hydrogel containing slide-ring polymers can be stretched to more than 10 times its initial length<sup>6</sup>; a tetra-poly(ethylene glycol) gel has a strength of  $\sim 2.6 \text{ MPa}$  (ref. 7). These gels deform elastically. An elastic gel is known to be brittle and notch-sensitive; that is, the stretchability and strength decrease markedly when samples contain notches, or any other features that cause inhomogeneous deformation<sup>19</sup>. A gel can be made tough and notch-insensitive by introducing energy-dissipating mechanisms. For example, a fracture energy of  $\sim 1,000 \text{ J m}^{-2}$  is achieved with a double-network gel, in which two networks—one with short chains, and the other with long chains—are separately crosslinked by covalent bonds<sup>11</sup>. When the gel is stretched, the short-chain network ruptures and dissipates energy<sup>20</sup>. But the rupture of the short-chain network causes permanent damage. After the first loading, the gel does not recover from this damage; thus, on subsequent loadings, the fracture energy is much reduced<sup>21</sup>. To enable recoverable energy-dissipating mechanisms, several recent works have replaced the sacrificial covalent bonds with non-covalent bonds. In a gel with a copolymer of triblock chains, for example, the end blocks of different chains form glassy domains, and the midblocks of different chains form ionic crosslinks<sup>22</sup>. When the gel is stretched, the glassy domains remain intact, while the ionic crosslinks break and dissipate energy. The ionic crosslinks then re-form during a time

interval after the first loading<sup>22</sup>. Recoverable energy dissipation can also be effected by hydrophobic associations<sup>17,18</sup>. When a gel made with hydrophobic bilayers in a hydrophilic polymer network is stretched, the bilayers dissociate and dissipate energy; on unloading, the bilayers re-assemble, leading to recovery<sup>17</sup>. However, previous studies along these lines have demonstrated fracture energy comparable to, or lower than, that of the double-network gels.

We have synthesized extremely stretchable and tough hydrogels by mixing two types of crosslinked polymer: ionically crosslinked alginate, and covalently crosslinked polyacrylamide (Fig. 1). An alginate chain comprises mannuronic acid (M unit) and guluronic acid (G unit), arranged in blocks rich in G units, blocks rich in M units, and blocks of alternating G and M units. In an aqueous solution, the G blocks in different alginate chains form ionic crosslinks through divalent cations (for example,  $\text{Ca}^{2+}$ ), resulting in a network in water—an alginate hydrogel. By contrast, in a polyacrylamide hydrogel, the polyacrylamide chains form a network by covalent crosslinks. We dissolved powders of alginate and acrylamide in deionized water. (Unless otherwise stated, the water content was fixed at 86 wt %.) We added ammonium persulphate as a photo-initiator for polyacrylamide, and N,N-methylenebisacrylamide as the crosslinker for polyacrylamide. After degassing the solution in a vacuum chamber, we added N,N,N',N'-tetramethylethylenediamine, at 0.0025 the weight of acrylamide, as the crosslinking accelerator for polyacrylamide, and calcium sulphate slurry ( $\text{CaSO}_4 \cdot 2\text{H}_2\text{O}$ ) as the ionic crosslinker for alginate. We poured the solution into a glass mould measuring  $75.0 \times 150.0 \times 3.0 \text{ mm}^3$ , covered with a 3-mm-thick glass plate. The gel was cured in one step with ultraviolet light for 1 hour (with 8 W power and 254 nm wavelength at 50 °C), and was then left in a humid box for 1 day to stabilize the reactions. After the curing step, we took the gel out of the humid box, and removed water on its surfaces using  $\text{N}_2$  gas for 1 minute.

The gel was glued to two polystyrene clamps, resulting in specimens measuring  $75.0 \times 5.0 \times 3.0 \text{ mm}^3$ . All mechanical tests were performed in air, at room temperature, using a tensile machine with a 500-N load cell. In both loading and unloading, the rate of stretch was kept constant at  $2 \text{ min}^{-1}$ . We stretched an alginate–polyacrylamide hybrid gel to  $>20$  times its original length without rupture (Fig. 2a,b). The hybrid gel was also extremely notch-insensitive. When we cut a notch into the gel (Fig. 2c) and then pulled it to a stretch of 17, the notch was dramatically blunted and remained stable (Fig. 2d). At a critical applied stretch, a crack initiated at the front of the notch, and ran rapidly through the entire sample (Supplementary Movie 1). Large, recoverable deformation is demonstrated by dropping a metal ball on a membrane of the gel fixed by circular clamps (Supplementary Movie 2). On hitting the membrane, the ball stretched the membrane greatly and then bounced back. The membrane remained intact, vibrated, and recovered its initial flat configuration after the vibration was damped out. A ball with greater kinetic energy, however, caused the membrane to rupture after large deformation (Supplementary Movie 3).

The extremely stretchable hybrid gels are even more remarkable when compared with their parents, the alginate and polyacrylamide

<sup>1</sup>School of Engineering and Applied Sciences, Harvard University, Cambridge, Massachusetts 02138, USA. <sup>2</sup>Department of Material Science and Engineering, Seoul National University, Seoul 151-742, South Korea. <sup>3</sup>Department of Mechanical Engineering and Materials Science, Duke University, Durham, North Carolina 27708, USA. <sup>4</sup>Wyss Institute for Biologically Inspired Engineering, Harvard University, Cambridge, Massachusetts 02138, USA. <sup>5</sup>Kavli Institute for Bionano Science and Technology, Harvard University, Cambridge, Massachusetts 02138, USA.

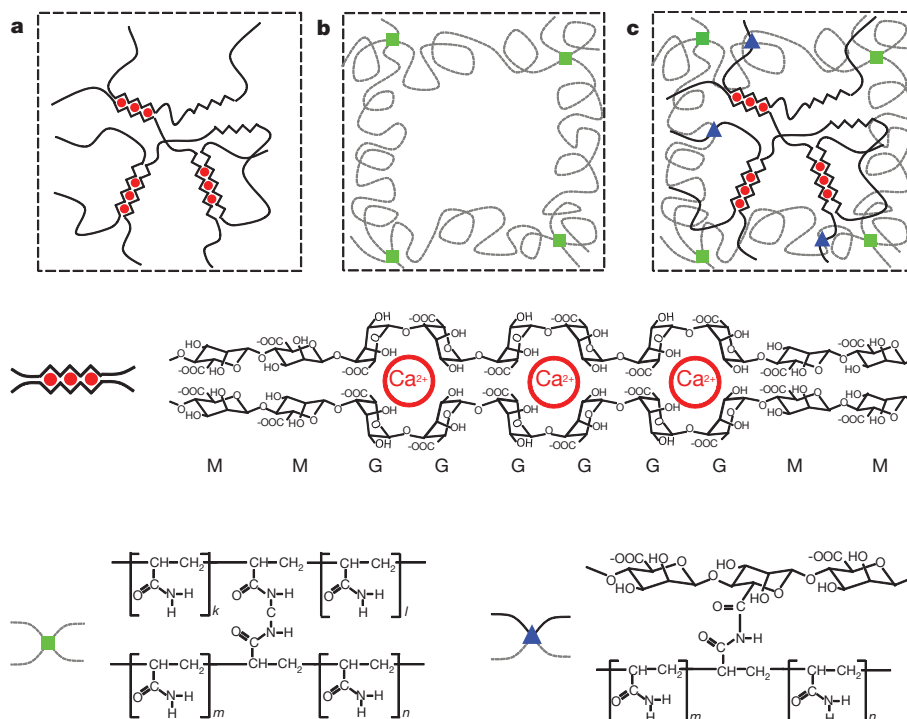


**Figure 1 | Schematics of three types of hydrogel.** **a**, In an alginate gel, the G blocks on different polymer chains form ionic crosslinks through  $\text{Ca}^{2+}$  (red circles). **b**, In a polyacrylamide gel, the polymer chains form covalent crosslinks through N,N-methylenebisacrylamide (MBAA; green squares). **c**, In an alginate-polyacrylamide hybrid gel, the two types of polymer network are intertwined, and joined by covalent crosslinks (blue triangles) between amine

groups (Fig. 3a). The amounts of alginate and acrylamide in the hybrid gels were kept the same as those in the alginate gel and polyacrylamide gel, respectively. When the stretch was small, the elastic modulus of the

hybrid gel was 29 kPa, which is close to the sum of the elastic moduli of the alginate and polyacrylamide gels (17 kPa and 8 kPa, respectively). The stress and stretch at rupture were, respectively, 156 kPa and 23 for the hybrid gel, 3.7 kPa and 1.2 for the alginate gel, and 11 kPa and 6.6 for the polyacrylamide gel. Thus, the properties at rupture of the hybrid gel far exceeded those of either of its parents.

Hybrid gels dissipate energy effectively, as shown by pronounced hysteresis. The area between the loading and unloading curves of a gel gives the energy dissipated per unit volume (Fig. 3b). The alginate gel exhibited pronounced hysteresis and retained significant permanent deformation after unloading. In contrast, the polyacrylamide gel showed negligible hysteresis, and the sample fully recovered its original length after unloading. The hybrid gel also showed pronounced hysteresis, but the permanent deformation after unloading was significantly smaller than that of the alginate gel. The pronounced hysteresis and relatively small permanent deformation of the hybrid gel were further demonstrated by loading several samples to large values of stretch before unloading (Fig. 3c).

After the first loading and unloading, the hybrid gel was much weaker if the second loading was applied immediately, and recovered somewhat if the second loading was applied 1 day later (Fig. 3d and Supplementary Fig. 1). We loaded a sample of the hybrid gel to a stretch of 7, and then unloaded the gel to zero force. The sample was

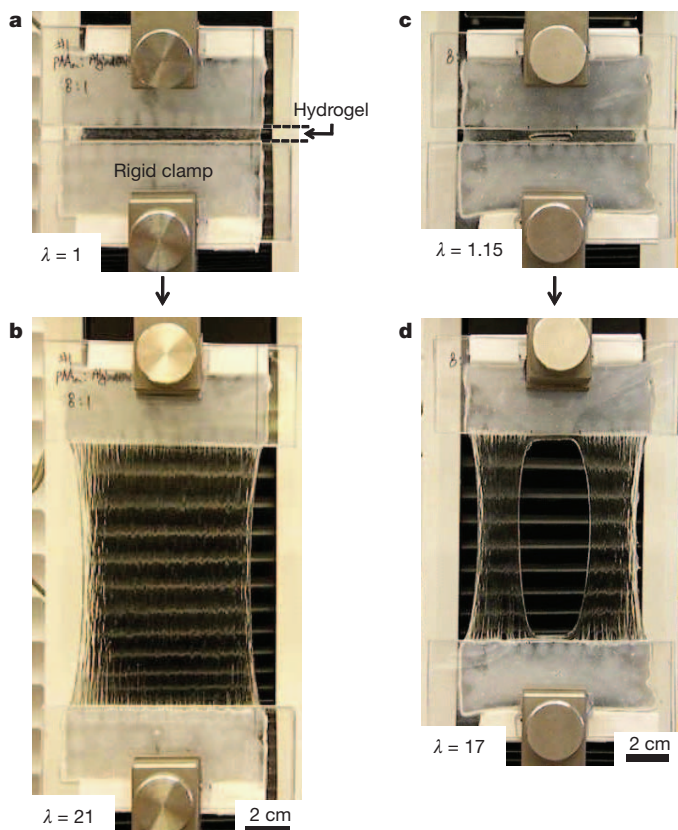


**Figure 2 | The hybrid gel is highly stretchable and notch-insensitive.** **a**, A strip of the undeformed gel was glued to two rigid clamps. **b**, The gel was stretched to 21 times its initial length in a tensile machine (Instron model 3342). The stretch,  $\lambda$ , is defined by the distance between the two clamps when the gel is deformed, divided by the distance when the gel is undeformed. **c**, A notch was cut into the gel, using a razor blade; a small stretch of 1.15 was used to make the notch clearly visible. **d**, The gel containing the notch was stretched to 17 times its initial length. The alginate/acrylamide ratio was 1:8. The weight of the covalent crosslinker, MBAA, was fixed at 0.0006 that of acrylamide; the weight of the ionic crosslinker,  $\text{CaSO}_4$ , was fixed at 0.1328 that of alginate.

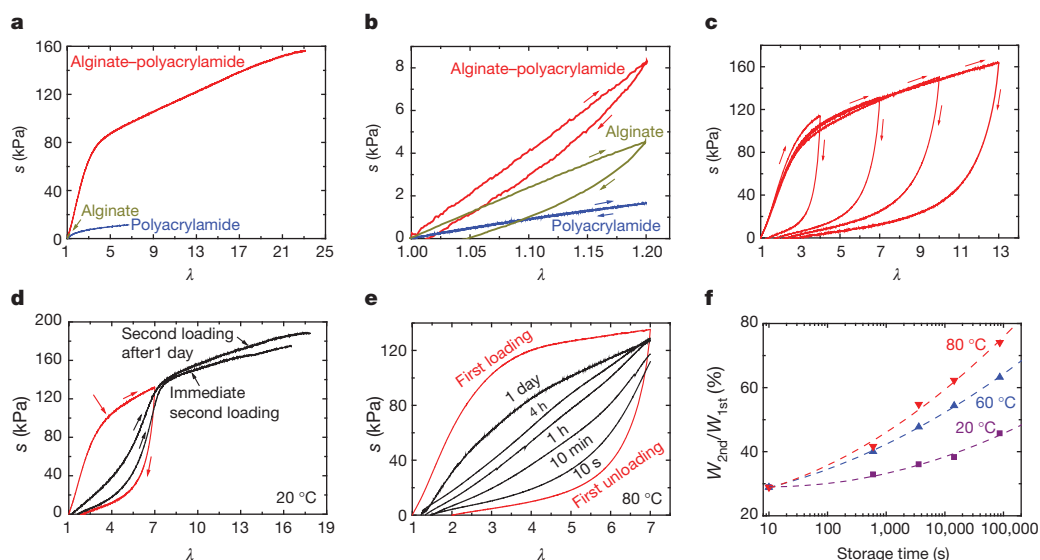


**Figure 3 | Mechanical tests under various conditions.** **a**, Stress–stretch curves of the three types of gel, each stretched to rupture. The nominal stress,  $s$ , is defined as the force applied on the deformed gel, divided by the cross-sectional area of the undeformed gel. **b**, The gels were each loaded to a stretch of 1.2, just below the value that would rupture the alginate gel, and were then unloaded. **c**, Samples of the hybrid gel were subjected to a cycle of loading and unloading of varying maximum stretch. **d**, After the first cycle of loading and

unloading (red curve), one sample was reloaded immediately, and the other sample was reloaded after 1 day (black curves, as labelled). **e**, Recovery of samples stored at 80 °C for different durations, as labelled. **f**, The work of the second loading,  $W_{2nd}$ , normalized by that of the first loading,  $W_{1st}$ , measured for samples stored for different durations at different temperatures. The alginate/acrylamide ratio was 1:8 for **a** and **b**, and 1:6 for **c**–**f**. Weights of crosslinkers were fixed as described in Fig. 2 legend.

then sealed in a polyethylene bag and submerged in mineral oil to prevent water from evaporating, and stored in a fixed-temperature bath for a prescribed time. The sample was then taken out of storage and its stress–stretch curve was measured again at room temperature. The internal damage was much better healed by storing the gel at an elevated temperature for some time before reloading (Fig. 3e and Supplementary Fig. 2). After storing at 80 °C for 1 day, the work on reloading was recovered to 74% of that of the first loading (Fig. 3f).

We prepared gels containing various proportions of alginate and acrylamide to study why the hybrids were much more stretchable and stronger than either of their parents. When the proportion of acrylamide was increased, the elastic modulus of the hybrid gel decreased (Fig. 4a). However, the critical stretch at rupture reached a maximum at 89 wt% acrylamide. A similar trend was observed for samples with notches (Fig. 4c). The fracture energy reached a maximum value of  $8,700 \text{ J m}^{-2}$  at 86 wt% acrylamide (Fig. 4d). The densities of ionic and covalent crosslinks also strongly affect the mechanical behaviour of the hybrid gels (Supplementary Figs 3, 4), as well as that of pure alginate gels (Supplementary Fig. 5) and pure polyacrylamide gels (Supplementary Fig. 6).

Our experimental findings provide insight into the mechanisms of deformation and energy dissipation in these gels. When an unnotched hybrid gel is subjected to a small stretch, the elastic modulus of the hybrid gel is nearly the sum of those of the alginate and polyacrylamide gels. This behaviour is also suggested by viscoelastic moduli determined for the hybrid and pure gels (Supplementary Fig. 7). Thus, in the hybrid gel the alginate and polyacrylamide chains both bear loads. Moreover, alginate is finely and homogeneously dispersed in the hybrid gel, as demonstrated by using fluorescent alginate and by measuring local elastic modulus with atomic force microscopy (Supplementary Fig. 8). The load sharing of the two networks may be achieved by entanglements of the polymers, and by possible covalent crosslinks formed between the amine groups on polyacrylamide chains and the carboxyl groups on alginate chains (Fig. 1, Supplementary Figs 9, 10). As the stretch increases, the alginate network unzips progressively<sup>23</sup>, while the polyacrylamide network remains intact, so that the hybrid gel exhibits pronounced hysteresis and little permanent deformation. As only the ionic crosslinks are broken, and

the alginate chains themselves remain intact, the ionic crosslinks can re-form, leading to the healing of the internal damage.

The giant fracture energy of the hybrid gel is remarkable, considering that its parents—the alginate and polyacrylamide gels—have fracture energies of  $10$ – $250 \text{ J m}^{-2}$  (Supplementary Figs 5, 6). The relatively low fracture energy of a hydrogel comprising a single network with covalent crosslinks is understood in terms of the Lake–Thomas model<sup>8</sup>. When the gel contains a notch and is stretched, the deformation is inhomogeneous; the network directly ahead of the notch is stretched more than elsewhere (Supplementary Fig. 11). For the notch

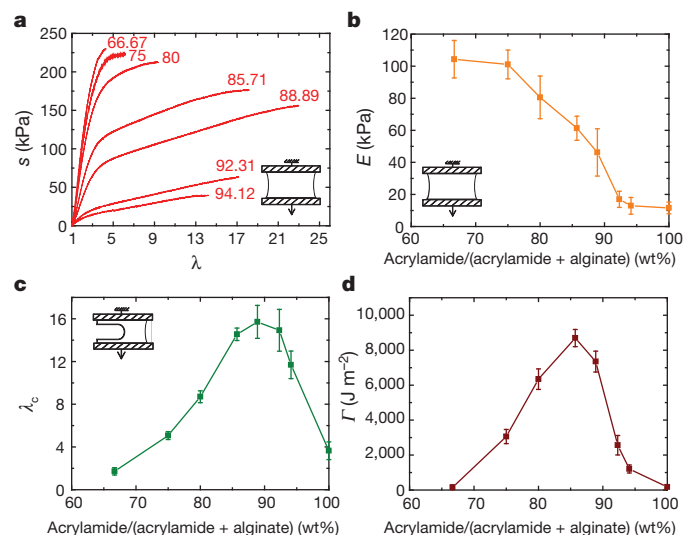


**Figure 4 | Composition greatly affects behaviour of the hybrid gel.** **a**, Stress–strain curves of gels of various weight ratios of acrylamide to (acrylamide plus alginate), as labelled. Each test was conducted by pulling an unnotched sample to rupture. **b**, Elastic moduli calculated from stress–strain curves, plotted against weight ratio. **c**, Critical stretch,  $\lambda_c$ , for notched gels of various weight ratios, measured by pulling the gels to rupture. **d**, Fracture energy,  $\Gamma$ , as a function of weight ratio. Weights of crosslinkers were fixed as described in Fig. 2 legend. Error bars show standard deviation; sample size  $n = 4$ .

to turn into a running crack, only the chains directly ahead of the notch need to break. Once a chain breaks, the energy stored in the entire chain is dissipated. In the ionically crosslinked alginate, fracture proceeds by unzipping ionic crosslinks and pulling out chains<sup>24</sup>. After one pair of G blocks unzip, the high stress shifts to the neighbouring pair of G blocks and causes them to unzip also (Supplementary Fig. 11). For the notch in the alginate gel to turn into a running crack, only the alginate chains crossing the crack plane need to unzip, leaving the network elsewhere intact. In both polyacrylamide gel and alginate gel, rupture results from localized damage, leading to small fracture energies.

That a tough material can be made of brittle constituents is reminiscent of transformation-toughening ceramics, and of composites made of ceramic fibres and ceramic matrices. The toughness of the hybrid gel can be understood by adapting a model well studied for toughened ceramics<sup>25</sup> and for gels of double networks of covalent crosslinks<sup>26,27</sup>. When a notched hybrid gel is stretched, the polyacrylamide network bridges the crack and stabilizes deformation, enabling the alginate network to unzip over a large region of the gel (Supplementary Fig. 11). The unzipping of the alginate network, in its turn, reduces the stress concentration of the polyacrylamide network ahead of the notch. The model highlights the synergy of the two toughening mechanisms: crack bridging and background hysteresis.

The idea that gels can be toughened by mixing weak and strong bonds has been exploited in several ways, including hydrophobic associations<sup>18</sup>, particle-filled gels<sup>7,15</sup> and supramolecular chemistry<sup>17,22</sup>. The fracture energy of the alginate–polyacrylamide hybrid gel, however, is much larger than previously reported values<sup>14,17,20,28</sup> for tough synthetic gels (100–1,000 J m<sup>-2</sup>), a finding that we attribute to how the alginate network unzips. Each alginate chain contains a large number of G blocks, many of which form ionic crosslinks with G blocks on other chains when enough Ca<sup>2+</sup> ions are present<sup>1</sup>. When the hybrid gel is stretched, the polyacrylamide network remains intact and stabilizes the deformation, while the alginate network unzips progressively, with closely spaced ionic crosslinks unzipping at a small stretch, followed by more and more widely spaced ionic crosslinks unzipping as the stretch increases.

Because of the large magnitude of the fracture energy and the pronounced blunting of the notches, we ran a large number of experiments to determine the fracture energy, using three types of specimen, as well as changing the size of the specimens (Supplementary Figs 12–16). The experiments showed that the measured fracture energy is independent of the shape and size of the specimens.

Our data suggest that the fracture energy of hydrogels can be greatly increased by combining weak and strong crosslinks. The combination of relatively high stiffness, high toughness and recoverability of stiffness and toughness, along with an easy method of synthesis, make these materials ideal candidates for further investigation. Further development is needed to relate macroscopically observed mechanical behaviour to microscopic parameters. Many types of weak and strong molecular integrations can be used, making hybrid gels of various kinds a fertile area of research. In many applications, the use of hydrogels is often severely limited by their mechanical properties. For example, the poor mechanical stability of hydrogels used for cell encapsulation often leads to unintended cell release and death<sup>29</sup>, and low toughness limits the durability of contact lenses<sup>30</sup>. Hydrogels of superior stiffness, toughness, stretchability and recoverability will improve the performance in these applications, and will probably open up new areas of application for this class of materials.

Received 16 February; accepted 10 July 2012.

- Lee, K. Y. & Mooney, D. J. Hydrogels for tissue engineering. *Chem. Rev.* **101**, 1869–1879 (2001).
- Qiu, Y. & Park, K. Environment-sensitive hydrogels for drug delivery. *Adv. Drug Deliv. Rev.* **53**, 321–339 (2001).
- Dong, L., Agarwal, A. K., Beebe, D. J. & Jiang, H. R. Adaptive liquid microlenses activated by stimuli-responsive hydrogels. *Nature* **442**, 551–554 (2006).

- Discher, D. E., Mooney, D. J. & Zandstra, P. W. Growth factors, matrices, and forces combine and control stem cells. *Science* **324**, 1673–1677 (2009).
- Calvert, P. Hydrogels for soft machines. *Adv. Mater.* **21**, 743–756 (2009).
- Okumura, Y. & Ito, K. The polyrotaxane gel: a topological gel by figure-of-eight cross-links. *Adv. Mater.* **13**, 485–487 (2001).
- Haraguchi, K. & Takehisa, T. Nanocomposite hydrogels: a unique organic-inorganic network structure with extraordinary mechanical, optical and swelling/de-swelling properties. *Adv. Mater.* **14**, 1120–1124 (2002).
- Lake, G. J. & Thomas, A. G. The strength of highly elastic materials. *Proc. R. Soc. A* **300**, 108–119 (1967).
- Simha, N. K., Carlson, C. S. & Lewis, J. L. Evaluation of fracture toughness of cartilage by micropenetration. *J. Mater. Sci. Mater. Med.* **14**, 631–639 (2003).
- Lake, G. J. Fatigue and fracture of elastomers. *Rubber Chem. Technol.* **68**, 435–460 (1995).
- Gong, J. P., Katsuyama, Y., Kurokawa, T. & Osada, Y. Double-network hydrogels with extremely high mechanical strength. *Adv. Mater.* **15**, 1155–1158 (2003).
- Huang, T. *et al.* A novel hydrogel with high mechanical strength: a macromolecular microsphere composite hydrogel. *Adv. Mater.* **19**, 1622–1626 (2007).
- Sakai, T. *et al.* Design and fabrication of a high-strength hydrogel with ideally homogeneous network structure from tetrahedron-like macromonomers. *Macromolecules* **41**, 5379–5384 (2008).
- Seitz, M. E. *et al.* Fracture and large strain behavior of self-assembled triblock copolymer gels. *Soft Matter* **5**, 447–456 (2009).
- Lin, W.-C., Fan, W., Marcellan, A., Hourdet, D. & Creton, C. Large strain and fracture properties of poly(dimethylacrylamide)/silica hybrid hydrogels. *Macromolecules* **43**, 2554–2563 (2010).
- Wang, Q. G. *et al.* High-water-content mouldable hydrogels by mixing clay and a dendritic molecular binder. *Nature* **463**, 339–343 (2010).
- Haque, M. A., Kurokawa, T., Kamita, G. & Gong, J. P. Lamellar bilayers as reversible sacrificial bonds to toughen hydrogel: hysteresis, self-recovery, fatigue resistance, and crack blunting. *Macromolecules* **44**, 8916–8924 (2011).
- Tuncaboylu, D. C., Sari, M., Oppermann, W. & Okay, O. Tough and self-healing hydrogels formed via hydrophobic interactions. *Macromolecules* **44**, 4997–5005 (2011).
- Hui, C.-Y., Jagota, A., Bennison, S. J. & Londono, J. D. Crack blunting and the strength of soft elastic solids. *Proc. R. Soc. Lond. A* **459**, 1489–1516 (2003).
- Yu, Q. M., Tanaka, Y., Furukawa, H., Kurokawa, T. & Gong, J. P. Direct observation of damage zone around crack tips in double-network gels. *Macromolecules* **42**, 3852–3855 (2009).
- Webber, R. E., Creton, C., Brown, H. R. & Gong, J. P. Large strain hysteresis and Mullins effect of tough double-network hydrogels. *Macromolecules* **40**, 2919–2927 (2007).
- Henderson, K. J., Zhou, T. C., Otim, K. J. & Shull, K. R. Ionically cross-linked triblock copolymer hydrogels with high strength. *Macromolecules* **43**, 6193–6201 (2010).
- Kong, H. J., Wong, E. & Mooney, D. J. Independent control of rigidity and toughness of polymeric hydrogels. *Macromolecules* **36**, 4582–4588 (2003).
- Baumberger, T. & Ronsin, O. From thermally activated to viscosity controlled fracture of biopolymer hydrogels. *J. Chem. Phys.* **130**, 061102 (2009).
- Evans, A. G. Perspective on the development of high-toughness ceramics. *J. Am. Ceram. Soc.* **73**, 187–206 (1990).
- Brown, H. R. A model of fracture of double network gels. *Macromolecules* **40**, 3815–3818 (2007).
- Tanaka, Y. A local damage model for anomalous high toughness of double-network gels. *Europhys. Lett.* **78**, 56005 (2007).
- Jackson, A. P. Measurement of the fracture toughness of some contact lens hydrogels. *Biomater.* **11**, 403–407 (1990).
- Hernández, R. M., Orive, G., Murua, A. & Pedraz, J. L. Microcapsules and microcarriers for in situ cell delivery. *Adv. Drug Deliv. Rev.* **62**, 711–730 (2010).
- Maldonado-Codina, C. & Efron, N. Impact of manufacturing technology and material composition on the mechanical properties of hydrogel contact lenses. *Ophthalmic Physiol. Opt.* **24**, 551–561 (2004).

Supplementary Information is available in the online version of the paper.

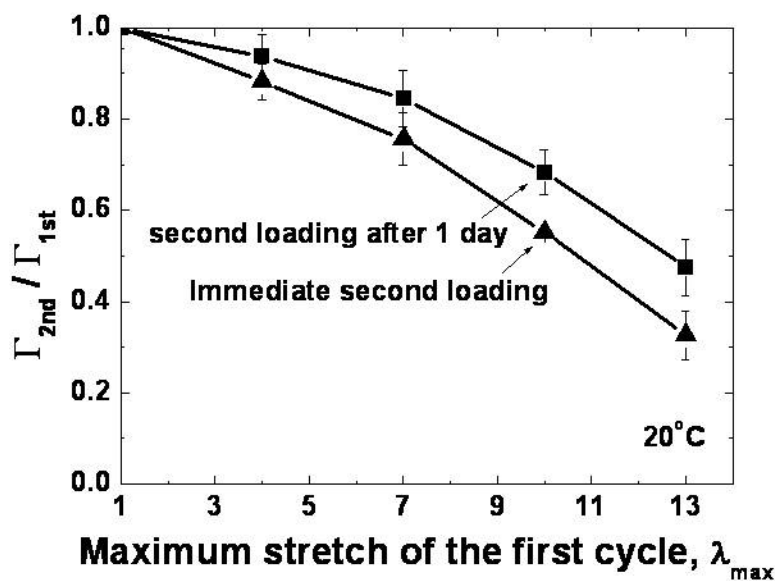
**Acknowledgements** The work at Harvard was supported by ARO (W911NF-09-1-0476), NSF (CMMI-0800161), DARPA (W911NF-10-1-0113), NIH (R37 DE013033) and MRSEC (DMR-0820484). X.Z. acknowledges the support of the NSF Research Triangle MRSEC (DMR-1121107) and Haythornthwaite Research Initiation grants. K.H.O. is supported by the National Research Foundation of Korea (NRF), funded by the Ministry of Education, Science and Technology (R11-2005-065). Z.S. acknowledges a sabbatical leave at the Karlsruhe Institute of Technology funded by the Alexander von Humboldt Award and by Harvard University.

**Author Contributions** J.-Y.S., X.Z., W.R.K.I., D.J.M., J.J.V. and Z.S. designed the study and interpreted the results. X.Z. developed the protocol for fabrication of the gels and prepared initial samples. J.-Y.S. and W.R.K.I. improved the protocol, and performed mechanical tests and recovery tests. J.-Y.S. obtained Fourier transform infrared spectra and performed thermogravimetric analysis. O.C. and J.-Y.S. conducted the experiment with fluorescent alginate and that using the atomic force microscope. K.H.O. contributed to the discussion of results. J.-Y.S., W.R.K.I. and Z.S. wrote the manuscript. All authors commented on the manuscript.

**Author Information** Reprints and permissions information is available at [www.nature.com/reprints](http://www.nature.com/reprints). The authors declare no competing financial interests. Readers are welcome to comment on the online version of the paper. Correspondence and requests for materials should be addressed to Z.S. ([suo@seas.harvard.edu](mailto:suo@seas.harvard.edu)).

## The effect of damage on reloading

The hybrid gel suffers internal damage after the first loading. To study the effect of the damage, we loaded a sample of the hybrid gel up to a certain stretch  $\lambda_{\max}$ , unloaded the gel to zero force, and followed with a second loading. The fracture energy measured on the second loading was reduced from that measured on the first loading (Supplementary Fig. 1). The amount of reduction increased with the maximum stretch of the first loading. The gel regained some fracture energy if the second loading was applied 1 day later. The fracture energy was determined by using a procedure described at the end of the supplementary information.

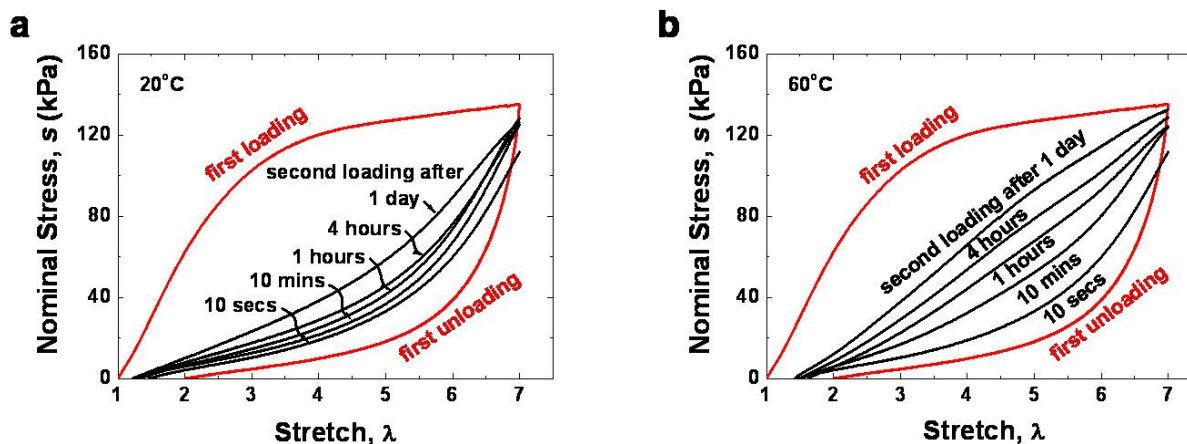


**Supplementary Figure 1 | Damage after the first cycle.** The hybrid gel was first loaded to a certain maximum stretch  $\lambda_{\max}$ , and was then unloaded to zero force, followed by a second loading. The fracture energy determined on the second loading  $\Gamma_{2nd}$  was reduced from that determined on the first loading  $\Gamma_{1st}$ . The alginate-to-acrylamide ratio was 1:6. The covalent crosslinker, MBAA, was fixed at 0.0006 the weight of acrylamide. The ionic crosslinker,  $\text{CaSO}_4$ , was fixed at 0.1328 the weight of alginate. (Error bars, S.D.; n=3).

## Recovery after the first loading: the effect of storage time and temperature

The recovery after the first loading takes time, and can be made faster by storing the gel in a hot bath. A sample of the hybrid gel was first loaded in tension to a stretch of 7, and was unloaded to zero force. The sample was then sealed in a polyethylene bag and submerged in mineral oil to prevent water from evaporation, and stored in a bath of a fixed temperature for a

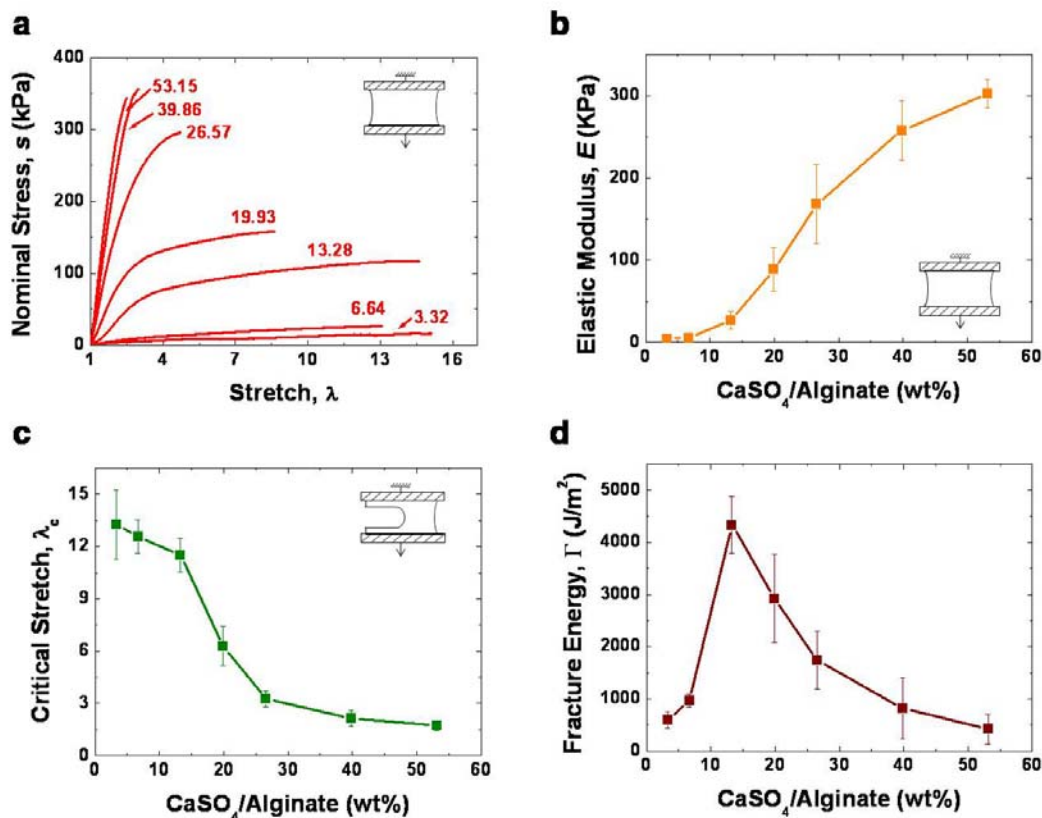
certain period of time. Afterwards the sample was taken out of storage and its stress-stretch curve was measured again at room temperature. Supplementary Fig. 2 shows the stress-stretch curve on the first loading and unloading, as well as the stress-stretch curves on the second loading after the sample was stored at certain temperatures for certain periods of time. In the second loading, the gel was weaker than the first loading. The extent of recovery increased with the temperature and time of storage.



**Supplementary Figure 2 | Recovery after the first loading.** Each hybrid gel sample was first loaded to a stretch of  $\lambda = 7$ , and then unloaded. The samples were then stored at a certain temperature for a period time, followed by a second loading at room temperature. Stress-stretch curves are shown for samples stored at: **a**, 20 °C; **b**, 60 °C. The alginate-to-acrylamide ratio was 1:6. The covalent crosslinker, MBAA, was fixed at 0.0006 the weight of acrylamide. The ionic crosslinker,  $\text{CaSO}_4$ , was fixed at 0.1328 the weight of alginate.

### Effect of the ionic crosslink density of alginate

To study the effect of the ionic crosslinks between alginate chains, we prepared hybrid gels with various concentrations of  $\text{CaSO}_4$  (Supplementary Fig. 3). For the unnotched samples, the stress needed to deform the gel increased with the concentration of  $\text{CaSO}_4$ . The small-strain elastic modulus increased with the concentration of  $\text{CaSO}_4$ . For the notched samples, however, the critical stretch for the notch to turn into a running crack decreased as the concentration of  $\text{CaSO}_4$  increased. The highest fracture energy was obtained for an intermediate concentration of  $\text{CaSO}_4$ . These trends are understood as follows. In the absence of  $\text{Ca}^{++}$ , alginate chains are not crosslinked, and bear no load, so that the hybrid gel exhibits a stress-stretch curve indistinguishable from that of the polyacrylamide gel, with large stretchability but low fracture energy. At a high concentration of  $\text{Ca}^{++}$ , alginate chains are densely crosslinked. Only a small zone around the root of the notch is stressed enough to break the alginate chains, so the fracture energy is low.



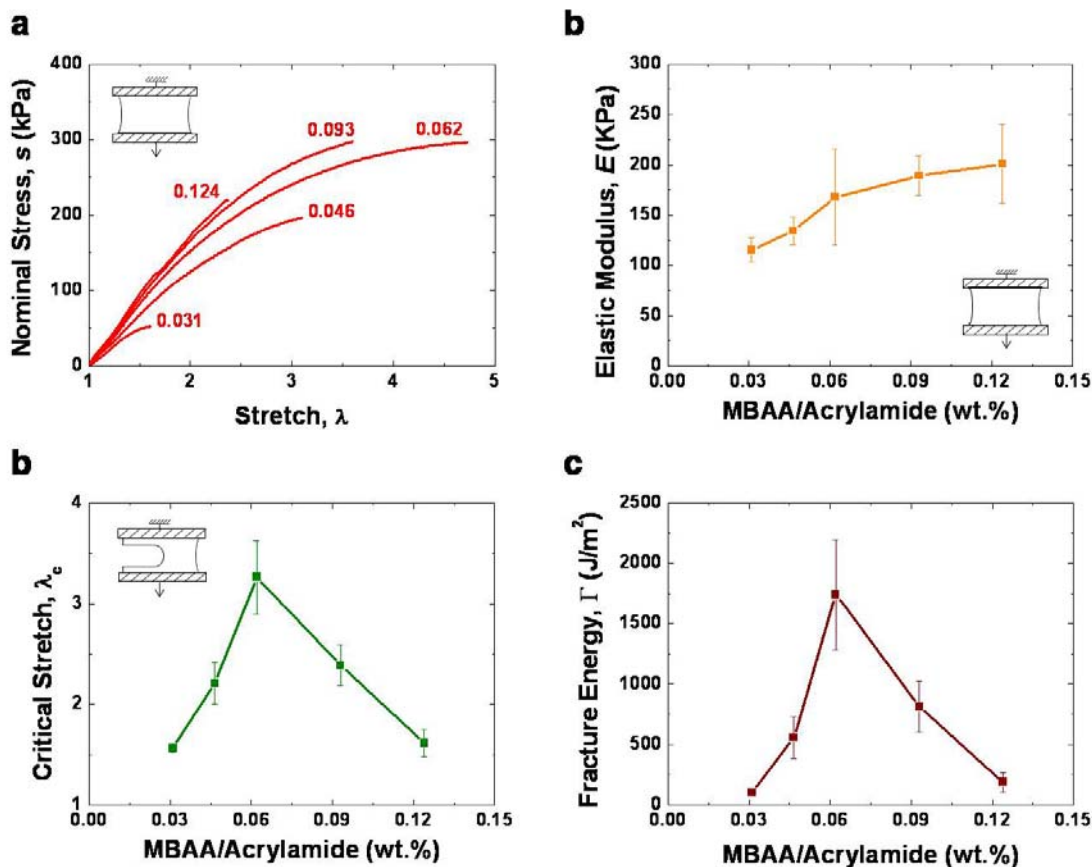
### Supplementary Figure 3 | The amount of ionic crosslinker, CaSO<sub>4</sub>, greatly affects the behavior of the hybrid gel.

**a**, Stress-strain curves were measured using unnotched samples of gels of various values of CaSO<sub>4</sub>/Alginate (wt%). **b**, Elastic moduli were determined by the initial slopes of the stress-strain curves. **c**, The critical stretches were measured using notched samples of gels. **d**, Fracture energy varies with the density of the ionic crosslinker. The weight ratio of alginate to acrylamide was fixed at 1:10, and the water content was fixed at 86 wt %. The covalent crosslinker, MBAA, was fixed at 0.0006 the weight of acrylamide. (Error bars, S.D.; n=3).

### Effect of the covalent crosslink density of polyacrylamide

To study the effect of the covalent crosslinks of polyacrylamide, we prepared hybrid gels with various concentrations of the crosslinker MBAA. Properties of these gels are shown in Supplementary Fig. 4. As the concentration of MBAA increased, the crosslink density of the polyacrylamide network increased. However, the stiffness of the hybrid gel increased only slightly. The concentration of MBAA did greatly affect the critical stretches of the notched samples. The highest fracture energy was obtained for an intermediate concentration of MBAA. This trend is understood as follows. When the covalent crosslink density is too high, each individual polyacrylamide chain between two crosslinks is short. When the chain breaks, the energy stored in the entire chain is dissipated. Consequently, shorter chains will lead to low fracture energy. In the other extreme, when the covalent crosslink density is too low, the polyacrylamide network becomes too compliant, incapable to stabilize the deformation of the gel.

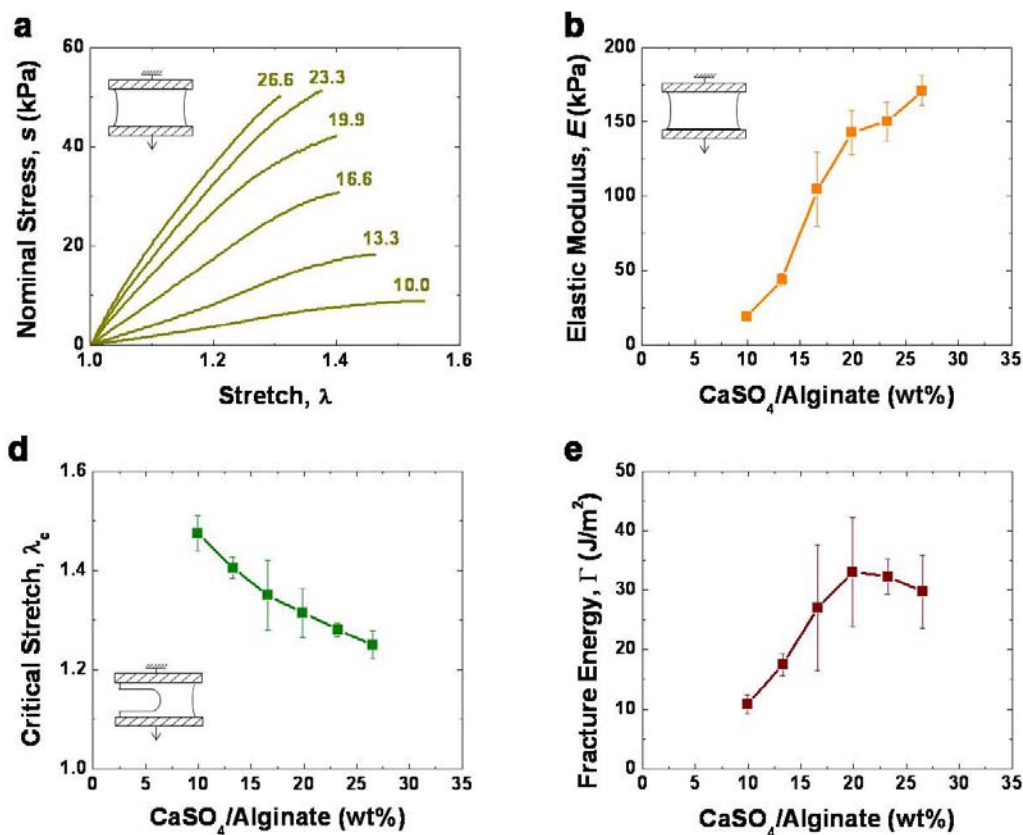
Consequently, deformation in a notched gel is localized: only a small part of the alginate network will unzip and dissipate energy.



**Supplementary Figure 4 | The amount of covalent crosslinker, MBAA, greatly affects the behavior of the hybrid gel.** **a**, Stress-strain curves were measured using unnotched samples of gels of various values of MBAA/Acrylamide (wt%). **b**, Elastic moduli were determined from the initial slopes of the stress-strain curves. **c**, The critical stretches were measured using notched samples of gels. **d**, Fracture energy varies with the concentration of the covalent crosslinker. The weight ratio of alginate to acrylamide was fixed at 1:10, and the water content was fixed at 86 wt %. The ionic crosslinker,  $\text{CaSO}_4$ , was fixed at 0.1328 the weight of alginate. (Error bars, S.D.;  $n=3$ ).

### The effect of the crosslinker density on alginate hydrogels

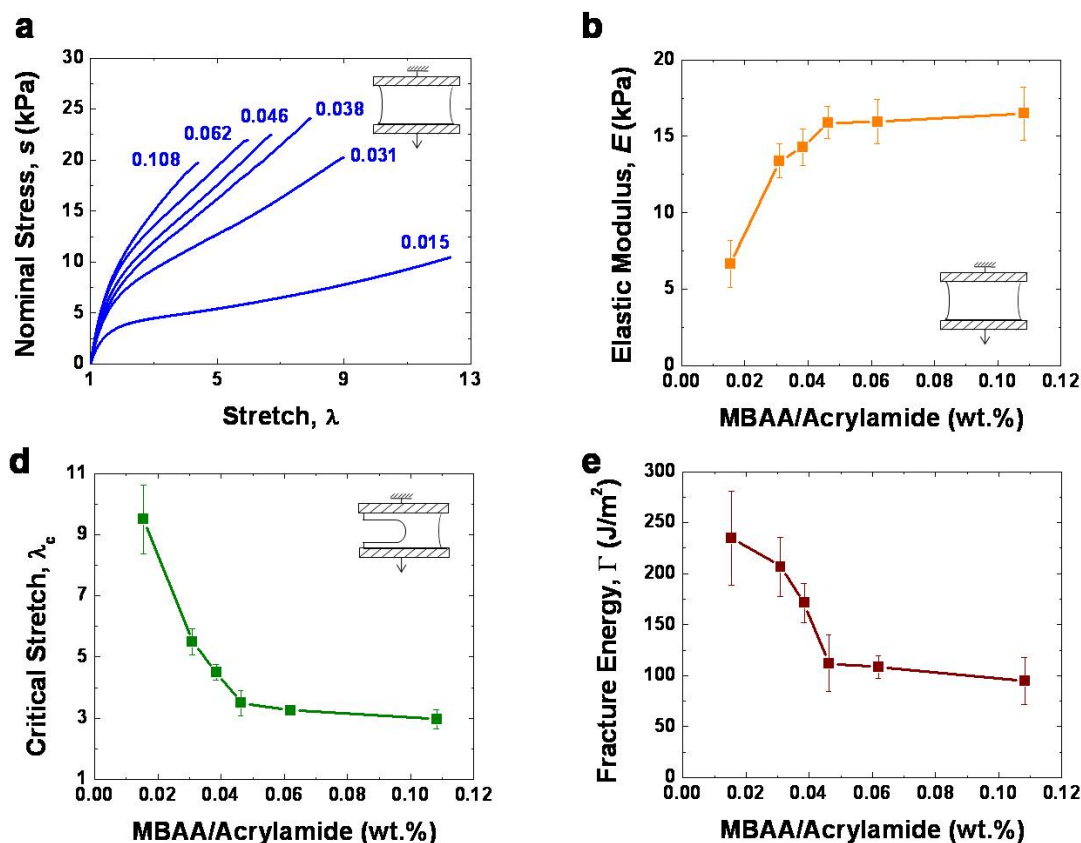
Mechanical properties were measured for alginate hydrogels of various  $\text{CaSO}_4$  concentrations (Supplementary Fig. 5). For the unnotched samples, the stress needed to deform the gel increased with the concentration of  $\text{CaSO}_4$ . For the notched samples, however, the critical stretch for the notch to turn into a running crack decreased as the concentration of  $\text{CaSO}_4$  increased. The highest fracture energy was obtained for an intermediate concentration of  $\text{CaSO}_4$ .



**Supplementary Figure 5 | The mechanical behavior of alginate hydrogels with various crosslinker densities.** **a**, Stress-strain curves were measured using unnotched samples of gels of various values of CaSO<sub>4</sub>/Alginate (wt%). **b**, Elastic moduli were calculated from stress-strain curves. **c**, The critical stretches were measured using notched samples of gels. **d**, Fracture energy varies with the density of the ionic crosslinker. (Error bars, S.D.;  $n=3$ ). Water content was fixed at 97 wt.%. (The solubility of alginate in water is less than 4 wt.%)

### The effect of crosslinker density on polyacrylamide hydrogels

Mechanical properties were measured for the polyacrylamide hydrogels of various MBAA concentrations (Supplementary Fig. 6). As the concentration of MBAA increased, the stiffness of the hybrid gel increased. However, the critical stretch of the notched samples decreased dramatically, the highest fracture energy was obtained for the minimum concentration of MBAA. Polyacrylamide single network gels with smaller than 0.015 wt.% MBAA concentration were only a viscous liquid after crosslinking.



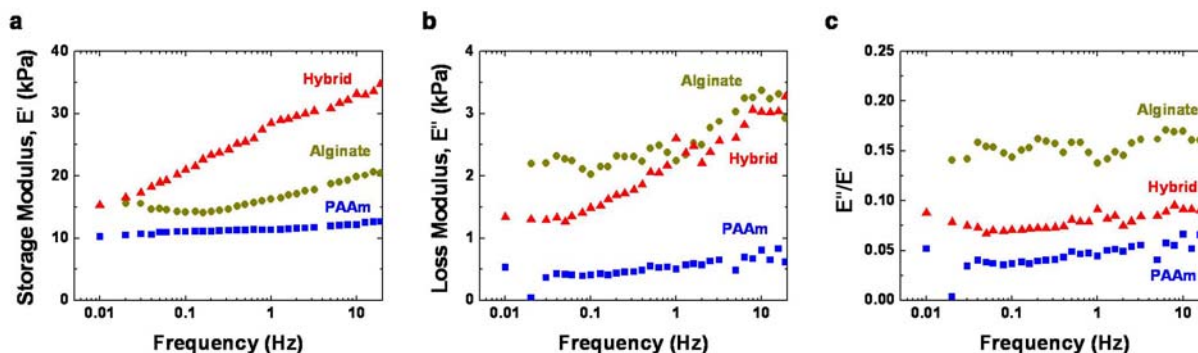
**Supplementary Figure 6 | The mechanical behavior of polyacrylamide hydrogels with various crosslinker densities.** **a**, Stress-strain curves were measured using unnotched samples of gels of various values of MBAA/Acrylamide (wt.%). **b**, Elastic moduli were calculated from stress-strain curves. **c**, The critical stretches were measured using notched samples of gels. **d**, Fracture energy varies with the concentration of the covalent crosslinker. Water content was fixed at 86.4 wt.%. (Error bars, S.D.;  $n=3$ ).

### Viscoelastic responses determined by dynamic mechanical analysis (DMA)

The viscoelastic responses of alginate, polyacrylamide, and alginate-polyacrylamide hybrid gels were determined by using DMA Q800 (TA Instruments). Compression frequency-sweep tests at 0.1% strain were carried out over the frequency range 0.01-30 Hz. Alginate gels with 97%, polyacrylamide gels with 86.4 wt.%, and alginate-polyacrylamide hybrid gels with 86.4 wt.% water concentration were used for this test. The polymer ratio of alginate-polyacrylamide hybrid gel is 1:6 of alginate to acrylamide. The covalent crosslinker, MBAA, was fixed at 0.0006 the weight of acrylamide for polyacrylamide gel and hybrid gel. The ionic crosslinker, CaSO<sub>4</sub>, was fixed at 0.1328 the weight of alginate for alginate gel and hybrid gel.

The storage modulus  $E'$  and the loss modulus  $E''$  for alginate, polyacrylamide, and hybrid gels were determined as the frequency changes (Supplementary Fig. 7). The ratio of  $E''/E'$  indicates the viscosity of the material. As expected, due to the unzipping behavior of the alginate network, alginate and hybrid gels show more viscous behavior than the polyacrylamide gels. Furthermore, alginate gels and alginate-polyacrylamide hybrid gels clearly show the

increase of  $E''$  at high frequency. The high frequency rise in  $E''$  reflects fast relaxation processes and is typical viscous behavior of gels formed by temporary (breakable) junction zones [31].

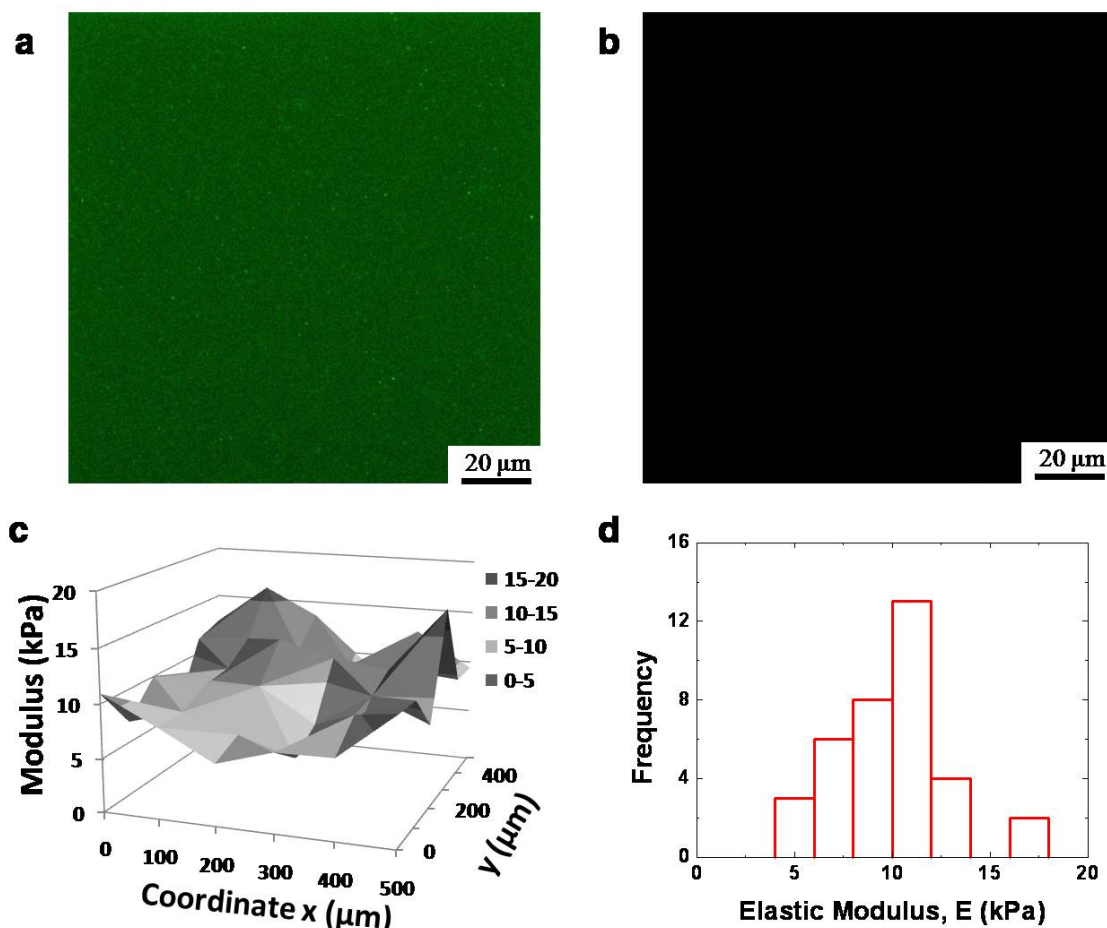


**Supplementary Figure 7 | Viscoelasticity of alginate, polyacrylamide, and hybrid gels. a, Storage modulus  $E'$ . b, Loss modulus  $E''$ . c, The ratio between  $E''$  and  $E'$ .**

### Homogeneity of hybrid gels

The homogeneity of alginate-polyacrylamide hybrid gels was investigated in two ways. First, the homogeneity of alginate networks in hybrid gels were tested using fluorescence images of hybrid gels which were fabricated from fluorescent alginate. Second, since the amount of calcium ion was strongly related to the elastic modulus of hybrid gels, the homogeneity of the calcium ions was explored by performing elastic modulus mapping of the surface of the hybrid gel. Alginate-polyacrylamide hybrid gels with 1:6 polymer ratio, 0.0006 MBAA concentration, 0.1328  $\text{CaSO}_4$  concentration, and 86.4 wt.% water concentration were used for these tests. Fluorescent alginate was prepared by coupling aminofluorescein (Sigma) to alginate polymers following same procedure as our previous work [2]. Fluorescence images were taken using a 1.40 NA 63X PlanApo oil immersion objective on a laser scanning confocal microscope (Zeiss LSM710). As demonstrated by a representative image (Supplementary Fig. 8a), the fluorescent alginate (shown in green) is fully interpenetrating and uniformly distributed within the hybrid gel.

The elastic modulus mapping is performed using atomic force microscope (Asylum-1 MFP-3D AFM System) with silicon nitride cantilever (Bruker AFM probes) with pyramid tipped probes. The stiffness of cantilevers is calibrated from thermal fluctuations ( $\sim 35$  pN/nm). To reduce the effect of the surface tension of the hydrogel, force measurements were performed in water with a 1000 nm/s sample surface movement. A  $500 \mu\text{m} \times 500 \mu\text{m}$  surface area of the hybrid gel is scanned and  $6 \times 6$  points are examined with a  $100 \mu\text{m}$  distance between each point. The elastic moduli were calculated from the relationship between indentation depth  $\delta$  and punch load  $F$  using the Hertzian model for a pyramid punch [3]. The resulting elastic moduli of hybrid gels and their distribution are plotted in Supplementary Fig. 8c and d, respectively. An average 10.0 kPa elastic modulus was obtained with 2.7 kPa standard deviation.



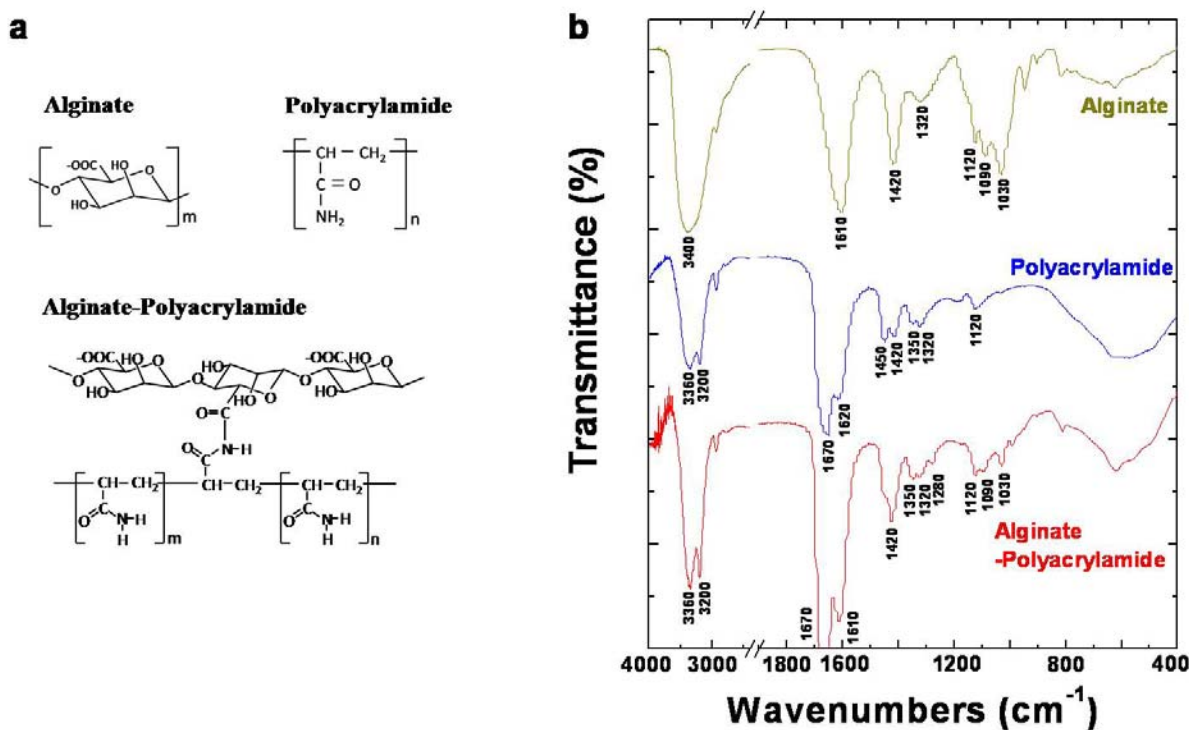
**Supplementary Figure 8 | Homogeneity of hybrid gel.** Fluorescence microscopy of hybrid gel mixed with fluorescent alginate (**a**) and without fluorescent alginate (**b**). **c**, Elastic modulus map of hybrid gel. **d**, Statistical plot of elastic modulus.

### Crosslinks between alginate and polyacrylamide.

As mentioned before, the stress-stretch curves of the hybrid gels clearly indicate that both alginate and polyacrylamide bear loads. The mechanism of load-transfer between the two types of polymers is unclear. To investigate possible crosslinks between the two types of polymers, we analyzed the Fourier Transform Infrared (FTIR) spectra of the alginate gel, polyacrylamide gel, and hybrid gel. Samples of the same thickness ( $\approx 100 \mu\text{m}$ ) were prepared for the alginate gel, the polyacrylamide gel, and the alginate-acrylamide hybrid gel. They were frozen at  $-20^\circ\text{C}$  and dried in vacuum chamber for 2 days to eliminate water molecules from the samples. FTIR spectra were recorded between  $4000$  and  $400 \text{ cm}^{-1}$  on a Nicolet 360 FTIR E.S.P. spectrometer.

The FTIR spectra of the three gels are shown in Supplementary Fig. 9. The alginate gel showed a broad peak near  $3400 \text{ cm}^{-1}$  for O-H stretching, one sharp peak at  $1620 \text{ cm}^{-1}$  for asymmetric COO- stretching, two peaks at  $1420$  and  $1320 \text{ cm}^{-1}$  for C-H deformation with secondary alcohols, and three peaks at  $1120$ ,  $1090$ , and  $1030 \text{ cm}^{-1}$  for asymmetric C-O-C

stretching, C-O stretching in CH-OH structure, and symmetric C-O stretching in C-O-C structure, respectively. The polyacrylamide gel exhibited bands at  $3360\text{ cm}^{-1}$  and  $3200\text{ cm}^{-1}$ , corresponding to a stretching vibration of N-H, and at  $1670\text{ cm}^{-1}$  for C=O stretching. The bands at  $1620\text{ cm}^{-1}$  (N-H deformation for primary amine),  $1450\text{ cm}^{-1}$  ( $\text{CH}_2$  in-plane scissoring),  $1420\text{ cm}^{-1}$  (C-N stretching for primary amide),  $1350\text{ cm}^{-1}$  (C-H deformation), and  $1120\text{ cm}^{-1}$  ( $\text{NH}_2$  in-plane rocking) were also detected. The spectra of the hybrid gel were characterized by comparing the presence of the absorption bands with the pure components. In the spectra of the hybrid gel, a new peak at  $1280\text{ cm}^{-1}$  for C-N stretching of secondary amide was created. Furthermore, the intensity of the absorption bands ( $1620$ ,  $1420\text{ cm}^{-1}$ ) which are related with primary amide, and the intensity of  $\text{NH}_2$  in-plane rocking peak ( $1120\text{ cm}^{-1}$ ) were decreased. Moreover, the intensities of O-H stretching peak ( $3400\text{ cm}^{-1}$ ), C-O stretching in CH-OH structure ( $1090\text{ cm}^{-1}$ ), and symmetric C-O stretching in C-O-C structure ( $1030\text{ cm}^{-1}$ ) were decreased. This result indicates new bonds formed between  $-\text{NH}_2$  groups of polyacrylamide and carboxyl groups of alginate.



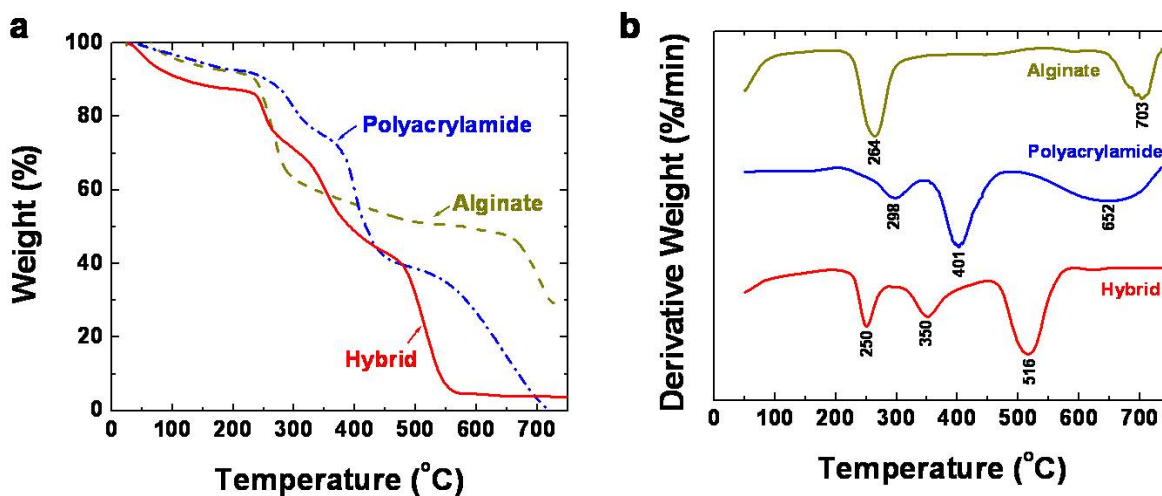
**Supplementary Figure 9 | Crosslinks between alginate and polyacrylamide.** **a**, Chemical structures of alginate and polyacrylamide, and suggested crosslinks between alginate and polyacrylamide. **b**, FTIR spectra alginate, polyacrylamide, and alginate-polyacrylamide hybrid.

### Thermogravimetric analysis (TGA)

To confirm the two gel networks were covalently coupled, the thermal degradation of the alginate, polyacrylamide, and alginate-polyacrylamide hybrid gels were studied using TGA Q5000 (TA Instruments), under a nitrogen atmosphere at a heating rate of  $10\text{ }^\circ\text{C}/\text{min}$ . Samples

were scanned from 40 to 750 °C. Alginate-polyacrylamide hybrid gel with the polymer ratio 1:6 of alginate to acrylamide was used for this test. Gel samples were frozen at -80 °C and dried in vacuum for a week, then the gels were ground with a mortar. Samples ranging between 4 and 8 mg in weight were tested in platinum pans.

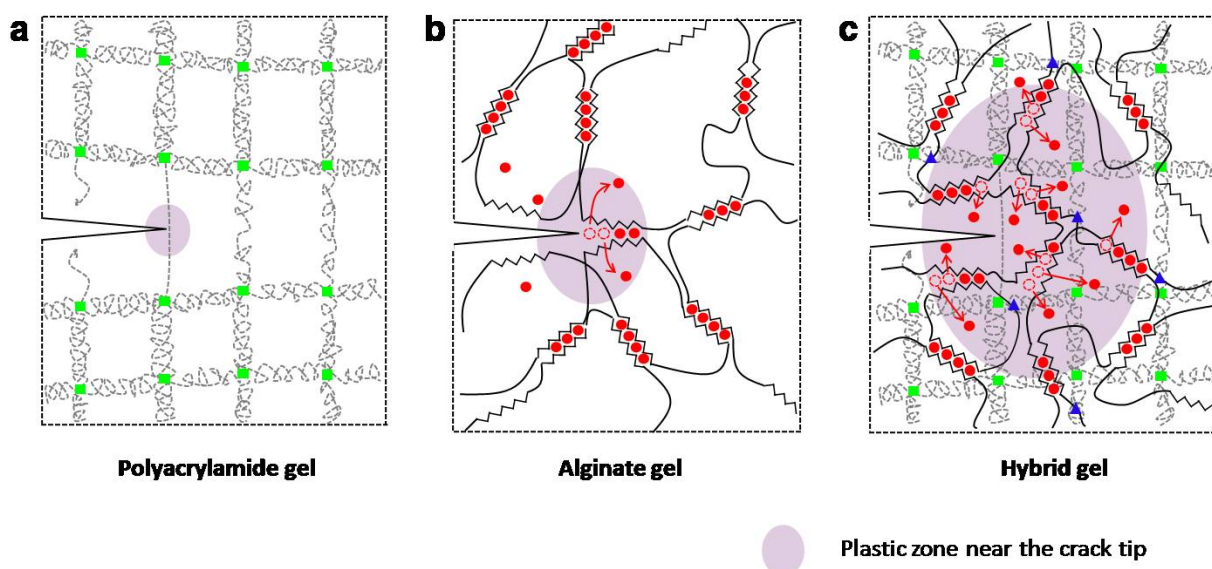
The integral results from the thermogravimetric analysis (TGA) are shown in Supplementary Fig. 10a, while the differential thermogravimetric data (DTG) are reported in Supplementary Fig. 10b, for alginate, polyacrylamide, and alginate-polyacrylamide hybrid gels. DTG data were deduced from TGA data by the derivative of the weight loss percent with respect to time. Each peak in DTG curves represents the temperature where the degradation rate is maximum for each degradation stage in the whole process. It is found that alginate has two pyrolysis stages, the first thermal degradation process occurred in the temperature range 225-300 °C. The weight loss in first stage is attributed to the degradation of the carboxyl group, as CO<sub>2</sub> is released. The second stage occurred in the range 650-740 °C, and is attributed to the depolymerization of polymer and formation of a carbonaceous residue, and finally yields CaCO<sub>3</sub> as char [34]. The thermal degradation of polyacrylamide occurs in three pyrolysis stages. In the temperature range 230-330 °C, one ammonia molecule is liberated for every two amide groups, resulting in the formation of imide [35]. Subsequently, thermal degradation of imides and breaking of the polymer backbone occurs as the second and third stages, as suggested by Burrows et al. Alginate-Polyacrylamide hybrid gel clearly shows three pyrolysis stages instead of the five stages which would result from the sum of the individual materials. Moreover the locations of the second and third stages of hybrid gel are shifted from the locations of the single networks. Complete chemical analysis from the degradation of hybrid gels is difficult. However, by comparing the trend with previous graft interpenetrating polymers [36-39], the reduced number of pyrolysis stages and shifted peak locations of DTG qualitatively support the formation of new covalent bonds between alginate and polyacrylamide.



**Supplementary Figure 10 | The thermal degradation of alginate, polyacrylamide, and alginate-polyacrylamide hybrid gels. a,** Data of thermogravimetric analysis (TGA). **b,** Data of differential thermogravimetry (DTG).

## Energy-dissipating mechanisms in three types of gels

When a notched gel is stretched, the deformation is inhomogeneous: the polymer chains directly ahead of the notch are stretched more than the chains elsewhere (Supplementary Fig. 11). For the notch in the polyacrylamide gel to turn into a running crack, only the chains directly ahead of the notch need to break. For the notch in the alginate gel to turn into a running crack, only the network directly ahead of the notch need to unzip. In either case, the gel is notch-sensitive because energy dissipates over a highly localized region: only a tiny fraction of the chains in the network—those crossing the crack plane—participate in energy dissipation. By contrast, in the hybrid gel, the number of chains that participate in energy dissipation is dramatically increased. For the notch in the hybrid gel to turn into a running crack, the chains directly ahead of the notch need to break. But before these chains break, the alginate network unzips over a large zone around the root of notch. This is likely the result of the efficient energy transfer between the two networks, due to their direct coupling, that results in alginate chains in a large zone being subjected to stress.



**Supplementary Figure 11 | Synergy between alginate and polyacrylamide.** **a**, In the polyacrylamide gel, for the notch to turn into a running crack, only the polyacrylamide chains crossing the crack plane need to break, and chains elsewhere remain intact. **b**, In the alginate gel, for the notch to turn into a running crack, only the ionic crosslinks for the chains crossing the crack need to break, and ionic crosslinks elsewhere remain intact. **c**, In the hybrid gel, the polyacrylamide chains bridge the crack and stabilize deformation in the background, the chemical interactions between the networks transfer the load over a large zone, and the ionic crosslinks between alginate chains break and provide inelastic deformation over this large zone around the root of the notch.

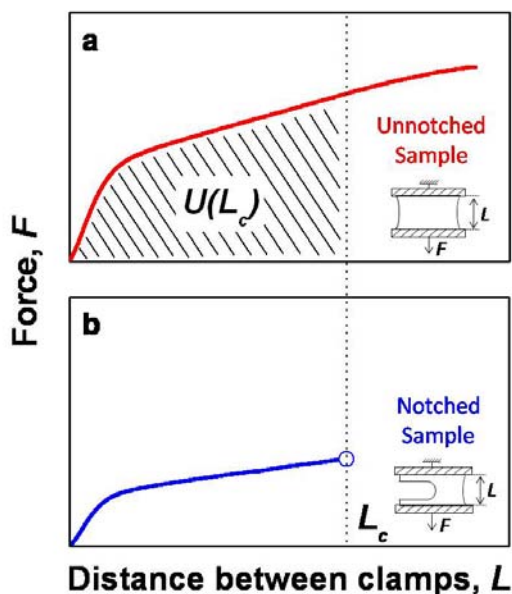
## Determination of fracture energy

We determined the fracture energy of a gel using a method introduced by Rivlin and Thomas [40]. To adapt the method to measure the fracture energy of an extremely stretchable gel, we separately pulled two samples of the same gel (Supplementary Fig. 12). One sample was

unnotched, and the other sample was notched. In the initial state when the gel was undeformed, each sample was of width  $a_0 = 75$  mm and thickness  $b_0 = 3$  mm, and the distance between the two clamps was  $L_0 = 5$  mm. The unnotched sample was pulled to measure the force-length curve. (To determine the fracture energy, it was unnecessary to pull the unnotched sample all the way to rupture.) When the two clamps were pulled to a distance  $L$ , the area beneath the force-length curve gave the work done by the applied force,  $U(L)$ . The notched sample was prepared by using a razor blade to cut into the gel a 40 mm-long notch. (The precise length of the notch was unimportant for this test.) The notched sample was pulled, and pictures were taken at a rate of  $\sim 30$  frames/sec to record the critical distance between the clamps,  $L_c$ , when the notch turned into a running crack. The fracture energy was calculated from

$$\Gamma = \frac{U(L_c)}{a_0 b_0}.$$

We verified this method with two other methods described by Rivlin and Thomas [S10]: the tensile test with multiple samples containing notches of various lengths, and the double-peeling test. Although the notch turned into a running crack when the sample was pulled to a huge length, the fracture energy determined by all three methods matched well. Even though the entire sample underwent inelastic deformation, the method is still expected to yield a valid test for fracture energy. The situation is similar to testing very ductile metals under large-scale yielding conditions [41].



**Supplementary Figure 12 | Experimental determination of fracture energy.** Two samples of the same gel were tested in tension. One sample was unnotched, and the other sample was notched. **a**, The unnotched sample was used to measure the force-length curve. The area beneath the force-length curve gave the work done by the force to the unnotched sample,  $U(L)$ . **b**, The notched sample was used to measure the critical distance between the clamps,  $L_c$ , when the notch turned into a running crack.

## Tensile test with samples of various crack lengths

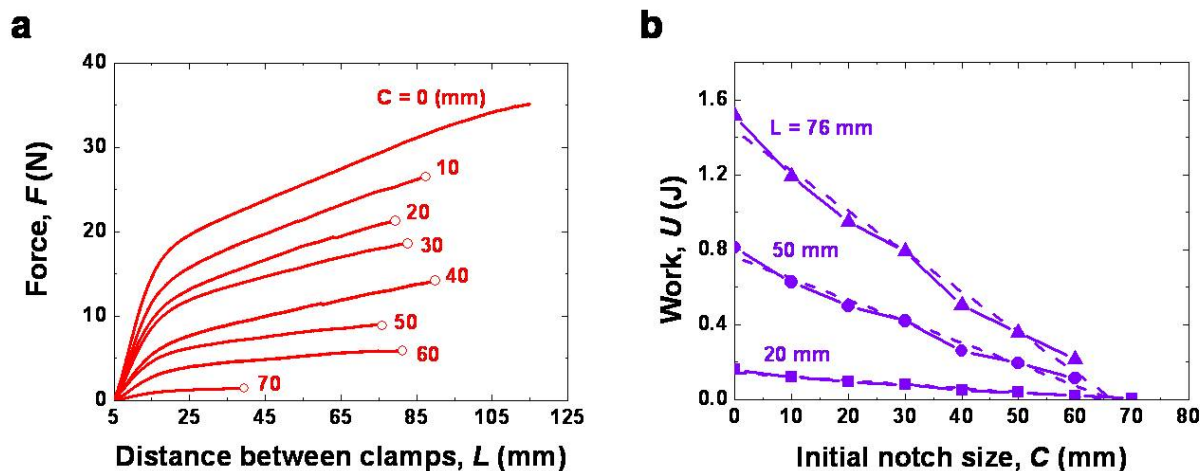
The pure-shear test was verified with two other tests: tensile test with samples of various crack lengths and double peeling test [S10]. Alginate-polyacrylamide hybrid gels with 1:8 polymer ratio, 0.0006 MBAA concentration, 0.1328 CaSO<sub>4</sub> concentration, and 86.4 wt.% water concentration were used for this verification.

First, tensile tests with various initial crack sizes were used to obtain fracture energy. Samples with dimensions  $L_0 = 5\text{mm}$ ,  $a_0 = 75\text{mm}$  and  $b_0 = 3\text{mm}$  were prepared with various crack lengths,  $C$ . The configuration of the test is the same as shown in Supplementary Fig. 12. Force-extension curves were obtained until the onset of crack propagation occurred.  $L$  is the change in distance between the clamps. The total energy  $U$  stored in the test piece at deformation  $L$  is obtained by measuring the area under the force-extension curve and  $U$  is plotted with the crack lengths,  $C$  as shown in Supplementary Fig. 13b. A suitable  $L$  value is selected in a way that it

corresponds to  $L$  of at least one fractured sample.  $\left(\frac{\partial U}{\partial C}\right)_L$  is calculated from the slope of the total energy vs crack length curve. Thus the fracture energy is given by,

$$\Gamma = \frac{1}{b_0} \left(\frac{\partial U}{\partial C}\right)_L$$

Using this method with  $L = 76\text{ mm}$ , the fracture energy obtained is  $7155 \pm 400 \frac{\text{J}}{\text{m}^2}$  which is comparable with the value  $7350 \text{ J/m}^2$  which is obtained from the pure-shear test.

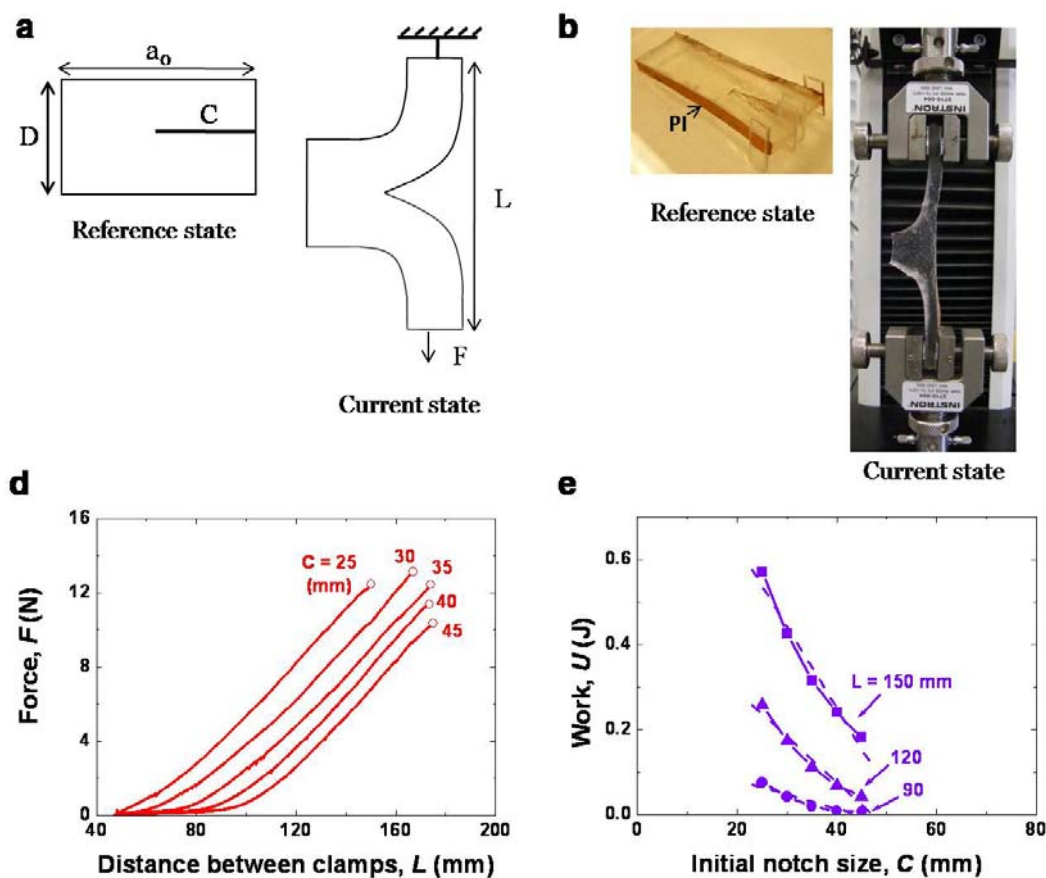


**Supplementary Figure 13 | Verification of the pure shear test method for extremely stretchy materials with tensile test with various crack lengths.** **a**, Force-extension curves for various crack lengths ( $C$ ) are plotted, the circles in each curve corresponds to the onset of crack propagation. **b**, The work done in deforming a test piece with various crack lengths was obtained from the area under the force-extension curve with the selected  $L$  values.

### Double peeling test

In order to verify the pure-shear test for extremely stretchy materials, we also used the double peeling test introduced by Rivlin and Thomas [S10]. Samples with dimensions  $D = 15\text{mm}$ ,  $a_0 = 80\text{mm}$  and thickness  $b_0 = 3\text{mm}$  were prepared with various crack lengths,  $C$  as shown in the schematic view in Supplementary Fig. 14a. To prevent the elongation of the arm of sample during stretching,  $200\ \mu\text{m}$  thick polyimide films were glued on both side of sample as shown in Supplementary Fig. 14b. Force-extension curves are obtained until the onset of crack propagation for various crack lengths as indicated Supplementary Fig. 14c. The total energy  $U$  stored in the test piece at deformation  $L$  is obtained by measuring the area under the force-extension curve and  $U$  is plotted with the crack lengths  $C$  as shown in Supplementary Fig. 14d. A

suitable  $L$  is selected as  $150\text{mm}$  and  $\left(\frac{\partial U}{\partial C}\right)_L$  is calculated from the slope of the total energy vs crack length curve. Fracture energy obtained from this method is  $7981 \pm 803 \frac{\text{J}}{\text{m}^2}$  which is comparable with the value of  $7350 \text{ J/m}^2$  obtained from the Rivlin-Thomas pure shear test.

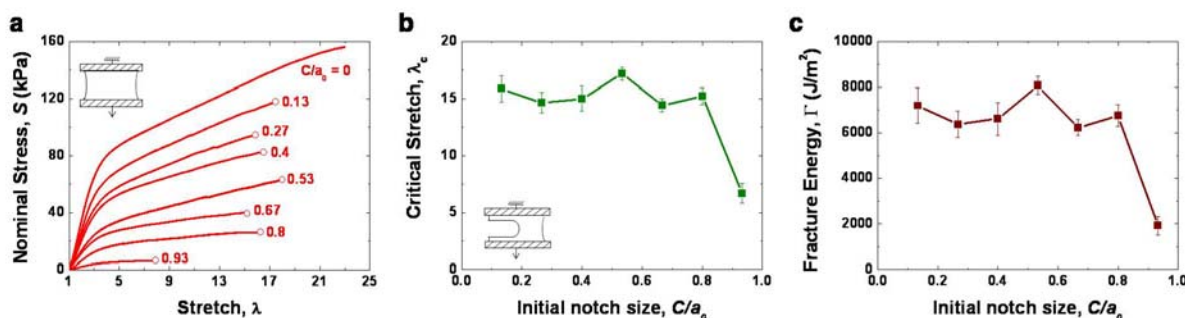


**Supplementary Figure 14 | Verification of the pure shear test method for extremely stretchy materials with double peeling test method.** **a**, Schematic figures of the reference state with dimensions  $D=15\text{mm}$ ,  $a_0=80\text{mm}$ ,  $b_0=3\text{mm}$  and current state after deformation are shown. **b**, Experimental figures of the double peeling test are shown. PI (Polyimide) strips are attached to the two ends of the specimen to control the deformation in the arms. **c**, Force-extension curves for various crack lengths ( $C$ ) are plotted. **d**, The work done in

deforming a test piece with various crack lengths were obtained from the area under the load-extension curve with selected  $h$  values.

### Crack length effect

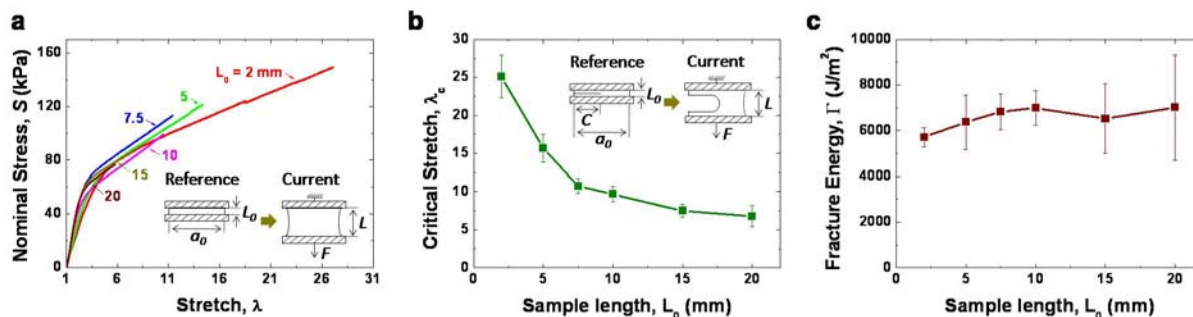
The effect of the initial crack length was investigated with various crack lengths. We prepared and tested samples of initial crack size  $C/a_0 = 0-0.93$ . The initial sample length  $L_0 = 5$  mm, width  $a_0 = 75$  mm, and thickness  $b_0 = 3$  mm were fixed for these tests. Alginate-polyacrylamide hybrid gels with 1:8 polymer ratio, 0.0006 MBAA concentration, 0.1328  $\text{CaSO}_4$  concentration, and 86.4 wt.% water concentration were used for these tests. Stress-stretch curves were measured with a various crack length until the crack propagation occurred as shown in Supplementary Fig. 15a. The onset crack propagation critical stretches were collected with various crack lengths and plotted in Supplementary Fig. 15b. The critical stretches do not vary much by initial crack lengths in the range of  $C/a_0 < 0.8$ . However, the critical stretch decreased to less than half of its value when the ligament length reaches less than 10% of the whole sample width. Fracture energy is calculated and plotted in Supplementary Fig. 15c as a function of crack lengths. As a result, we obtained a consistent fracture energy within the range of  $C/a_0 < 0.8$ .



**Supplementary Figure 15 | Effect of initial crack length on toughness value. a,** Stress-stretch curves for various initial crack lengths, the circles denote the onset of crack propagation. **b,** Critical stretch of the sample with various crack lengths normalized to sample width. **c,** Fracture toughness of the sample as a function of pre-crack length. (Error bars, S.D.;  $n=3$ ).

### Sample size effect

To ascertain that the fracture energy is independent of sample size, we prepared and tested samples of initial lengths  $L_0 = 2-20$  mm (Supplementary Fig. 12). The smallest sample,  $L_0 = 2$  mm was limited by our experimental setup. The initial sample width  $a_0 = 75$  mm, thickness  $b_0 = 3$  mm, and notch size  $C \approx 0.5a_0$  were fixed for these tests. While the critical stretch decreased with the sample size, the fracture energy remained nearly a constant. Even though the entire sample underwent inelastic deformation, the method yielded a valid test for fracture energy. The situation is similar to testing very ductile metals under large-scale yielding conditions [41]. This experiment indicates that the intrinsic length scale associated with fracture energy is below the minimum sample size used here,  $L_0 = 2$  mm. Alginate-polyacrylamide hybrid gels with 1:8 polymer ratio, 0.0006 MBAA concentration, 0.1328  $\text{CaSO}_4$  concentration, and 86.4 wt.% water concentration were used for these tests.



**Supplementary Figure 16 | Effect of sample length on toughness value.** **a**, Stress-stretch curves for various crack lengths, the circles denote the onset of crack propagation. **b**, Critical stretch of the sample with various sample lengths normalized with sample width. **c**, Fracture toughness of the sample as a function of sample length. (Error bars, S.D.;  $n=3$ ).

## References

31. Annable T., Buscall B., Ettelaie R., and Whittlestone D. The rheology of solutions of associating polymers: comparison of experimental behavior with transient network theory. *J. Rheology* **37**, 695-726 (1993).
32. Kong H. J., Kim C. J., Huebsch N., Weitz D., and Mooney D. J. Noninvasive probing of the spatial organization of polymer chains in hydrogels using fluorescence resonance energy transfer (FRET). *J. Am. Chem. Soc.* **129**, 4518-4519 (2007).
33. Bilodeau G. G. Regular pyramid punch problem. *J. Applied Mech.* **59**, 519-523 (1992).
34. Liang C. X., Hirabayashi K. Improvements of the physical-properties of fibroin membranes with sodium alginate. *J. App. Poly. Sci.* **45**, 1937-1943 (1992).
35. Burrows H. D., Ellis H. A. and Utah S. I. Adsorbed metal ions as stabilizers for the thermal degradation of polyacrylamide. *Polymer* **22**, 1740-1744 (1981).
36. Silva D. A., Paula R. C. M., Feitosa J. P. A. Graft copolymerization of acrylamide onto cashew gum. *European Polymer Journal* **43**, 2620-2629 (2007).
37. Raymond M.-P., Bui V. T. Epoxy/Castor Oil Graft Interpenetrating Polymer Networks. *J. App. Poly. Sci.* **70**, 1649-1659 (1998).
38. Athawale V. D., Lele V. Thermal studies on granular maize starch and its graft copolymers with vinyl monomers. *Starch* **52**, 205-213 (2000)
39. Xue T. J., Wilkie C. A. Thermal degradation of poly(styrene-g-acrylonitrile). *Polymer degradation and stability* **56**, 109-113 (1997).
40. Rivlin, R. S. & Thomas, A. G. Rupture of rubber. I. Characteristic energy for tearing. *J. Polym. Sci.* **10**, 291-318 (1953).
41. Begley, J.A. & Landes, J.D. The J integral as a fracture criterion. *Fracture Toughness, Proceedings of the 1971 National Symposium on Fracture Mechanics, Part II, ASTM STP 514*, American Society for Testing and Materials, pp. 1-20 (1972).

### Supplementary Movie 1

This movie shows a crack initiating at the front of a blunted notch, and running rapidly across the sample. A notch was cut into a sample of the hybrid gel. When the gel was stretched, the notch blunted dramatically and remained stable. At a critical applied stretch, a crack initiated at the front of the notch, and ran rapidly through the entire sample. In the undeformed state, the front of the notch was much smaller than the length of the notch. In the deformed state, just before the initiation of the crack, the front was stretched so much that different locations along the front were clearly visible. In this work, however, no effort was made to identify the exact location where the crack was initiated. The alginate-to-acrylamide ratio was 1:8. The covalent crosslinker, MBAA, was fixed at 0.0006 the weight of acrylamide. The ionic crosslinker,  $\text{CaSO}_4$ , was fixed at 0.1993 the weight of alginate. The tests were performed in air, at room temperature, using a tensile machine (Instron model 3342) with a 500-N load cell. The rate of stretch was kept constant at 2 per minute. The real-time movie was recorded at a typical rate of 30 frames/sec.

### Supplementary Movie 2

This movie demonstrates large, recoverable deformation when a metal ball drops on a membrane of the hybrid gel. The membrane, thickness 1 mm, was glued to two clamps of polyacrylate with a circular opening, inner diameter 7 cm. A stainless steel ball, diameter 2.54 cm and mass 64 g, was dropped from a high of 1.86 m. Upon hitting the membrane, the ball stretched the membrane greatly, and then bounced back. The membrane remained intact, vibrated, and recovered its initial flat configuration after the vibration was damped out. The alginate-to-acrylamide ratio was 1:4. The covalent crosslinker, MBAA, was fixed at 0.0006 the weight of acrylamide. The ionic crosslinker,  $\text{CaSO}_4$ , was fixed at 0.1328 the weight of alginate. High-speed camera (Vision Research Phantom V711) recorded movies at a typical rate of 6000 frames per second, and a typical exposure time of 160  $\mu\text{s}$ .

### Supplementary Movie 3

This movie shows large deformation and rupture when a metal ball drops on a membrane of the hybrid gel. The experimental setup was the same as that in Supplementary Movie 2, except for the size of the steel ball and thickness of gel membrane. A steel ball, diameter 5.08 cm and mass 524 g, was dropped from a high of 1.86 m, and the membrane of the gel used was 2 mm thick. Upon hitting the membrane, the ball stretched the membrane greatly, and caused the membrane to rupture.